AN ABSTRACT OF THE THESIS OF

Nicolai Thum for the degree of Master of Science in Atmospheric Sciences presented on February 22, 2001. Title: Air-Sea Heat Exchange Along the Northern Sea Surface Temperature Front in the Eastern Tropical Pacific.

Redacted for privacy

Abstract approved: _____

Steven K. Esbensen

The atmospheric response to the oceanic forcing in the eastern Pacific along the northern equatorial sea surface temperature (SST) front is investigated in terms of sensible and latent heat flux during the 6-month period 28 July 1999 through 27 January 2000. Of particular interest is the atmospheric boundary layer (ABL) response to oceanic Tropical Instability Waves (TIWs) that distort the SST front during May through January in normal years. In previous studies, time series of boundary layer properties clearly show the influence of TIWs but the relationship to spatial patterns of SST and wind stress has been inferred only from sparse in situ data.

In this study, satellite observations are used to composite in situ data from moorings to compensate for the lack of a spatially dense mooring array. The variability in the position of the SST front caused by propagating TIWs enables fixed mooring locations to measure the atmospheric boundary layer (ABL) response from a large range of locations relative to the front. The satellite data enable determination of the precise location of the mooring relative to the front. The advantage of this strategy is the recurring measurement of the ABL response to the SST front over the six month period considered here.

The results indicate that the TIW-induced perturbations of sensible and latent heat flux are spatially shifted in phase towards the east relative to the perturbations of SST. The maximum fluxes are not centered directly over the warmest water, but are shifted towards the portion of the frontal region where a disequilibrium boundary layer is expected due to the advection of colder air from the equatorial region. The changes of sensible and latent heat fluxes across the SST front have magnitudes of about 11 Wm^{-2} and 126 Wm^{-2}, respectively.

The sensible and latent heat flux patterns are interpreted in two complementary ways: (1) as an atmospheric response to the change of oceanic forcing as air flows across the SST front; and (2) as the atmospheric response to westward propagating TIWs along the SST front.

Air-Sea Heat Exchange Along the Northern Sea Surface Temperature Front in the Eastern Tropical Pacific

by

Nicolai Thum

A THESIS

submitted to

Oregon State University

in partial fulfillment of
the requirements for the
degree of

Master of Science

Completed February 22, 2001
Commencement June 2001

Master of Science thesis of Nicolai Thum presented on February 22, 2001

APPROVED:

Redacted for privacy

Major Professor, representing Atmospheric Sciences

Redacted for privacy

Dean of the College of Oceanic and Atmospheric Sciences

Redacted for privacy

Dean of the Graduate School

I understand that my thesis will become part of the permanent collection of Oregon State University libraries. My signature below authorizes release of my thesis to any reader upon request. Redacted for privacy

Nicolai Thum, Author

ACKNOWLEDGMENTS

I would like to express my full appreciation for the guidance and advising of Dr. Steve Esbensen. He has trusted my abilities and provided me fantastic opportunities. His encouragement and extensive reviews were instrumental in the completion of this thesis.

I would also like to thank the members of my committee: Dudley B. Chelton, Michael H. Freilich, Larry Mahrt and Michael M. Lerner for their time, support and careful editing.

Thanks also to Dean Vickers and Michael Schlax for their technical support.

I thank my parents Margret and Herbert Thum and my sister Corina for being supportive of all my efforts, for their love and encouragement.

Thanks for the friendship of Claudius, Jennifer, Carrie, Yves, Joern, Kim, Brandy, James, François, Renellys, Sebastian, Guillaume, Nicolas, Debbie, Claudia, Bertrand, Reina and Mark.

This work was supported by NOAA Office of Global Programs and NASA Jet Propulsion Laboratories.

CONTRIBUTION OF AUTHORS

Dr. Steven K. Esbensen and Dr. Dudley B. Chelton were involved as thesis advisers in the analysis and writing of this thesis. Dr. Michael J. McPhaden provided the TAO data and helpful comments on the manuscript

TABLE OF CONTENTS

LIST OF FIGURES

LIST OF FIGURES (Continued)

AIR-SEA HEAT EXCHANGE ALONG THE NORTHERN SEA SURFACE TEMPERATURE FRONT IN THE EASTERN TROPICAL PACIFIC

1 INTRODUCTION

Air-sea interaction in the eastern tropical Pacific Ocean has been a topic of great interest for many years because of its significance to the global climate. In the atmosphere, the equatorial region between 15°N and 15°S is characterized by the confluence of the northern and southern hemisphere trade-wind regimes into the inter-tropical convergence zone (ITCZ). The ITCZ undergoes an annual march with the band of strongest convection in the southern hemisphere in March, migrating northward during the transition to northern hemisphere summer and remaining between 5° and 10°N until almost the end of the year (Mitchell and Wallace 1992). In the Eastern Pacific upper ocean the equatorial region is dominated by the upwelling of cold water along the South American coast during May through January. The cold upwelled water migrates westward along the equator and defines the equatorial cold tongue which extends to about 160°W and some 5 degrees to the north and the south.

Although the annual cycle of incident solar radiation is symmetric about the equator, the mean atmospheric circulation in the eastern tropical Pacific is asymmetric and the region of deepest convection is found north of the equator in the climatological average. The southeasterly trade winds cross the equator

and turn anticyclonically toward Mexico and Central America, and converge in the ITCZ. The location of the ITCZ and the structure of the cold-tongue/ITCZ complex have been subjects of numerous studies (e.g., Lindzen and Nigam 1987, Mitchell and Wallace 1992, Philander et al. 1996) and there is ongoing debate whether the large scale dynamics are determining the location of convection or the convection and sea surface temperature are determining the location of the ITCZ (see discussion in Tomas and Webster 1997).

The atmospheric boundary layer (ABL) from the equator to 5°N is an important component of the cold-tongue/ITCZ complex because of (1) ITCZ inflow effects through air mass modification and (2) wind stress and heat flux forcing of the upper ocean. This particular region of the eastern tropical Pacific is characterized by a strong SST gradient defining the northern flank of the cold-tongue and by the oceanic TIWs perturbing the SST front during May through January (see Fig. 1.1). TIWs are generated by the strong shear in the equatorial oceanic current system. These oceanic waves propagate westward with phase speeds of ≈ 0.5 ms^{-1}, periods of 20 to 40 days and wavelengths of 1000–2000 km (Qiao and Weisberg 1995).

The prevailing wind in the ABL across the northern SST front during the TIW season from May through January is southeasterly, from cold to warm water. The wind direction suggests advection of cold boundary layer air across the sharp SST front into the region of warm surface water. In this scenario, the air-sea temperature difference is increased over the warm water, indicating strong air-sea interactions. Bond (1992) suggested that air-sea fluxes lead to a reduction of low-level wind shear north of the cold tongue. This reduction of wind shear is thought to be at least partly caused by a reduction of static stability and enhanced horizontal momentum mixing on the warm side of the front. The

enhanced downward mixing of vertical momentum accelerates the wind to the north of the front and the pattern of wind stress changes significantly across the SST front. Mean values over a 3 month period from July through October 1999 of less than 0.02 N m^{-2} are found over the cold tongue, increasing to more than 0.08 N m^{-2} over the warm water (Chelton et al. 2001).

Such coupling between the atmospheric boundary layer and the TIW SST patterns should result in distinctive patterns of wind stress and other meteorological features that propagate slowly to the west with the SST perturbations. Using satellite observations of low-level cloud coverage, Deser et al. (1993) found that large values of cloud reflectivity were observed over and upstream of the warm SST anomalies. Using satellite observations of SST and wind speed, Xie et al. (1998) found that the wind divergence field was highly correlated with the TIW SST anomaly patterns, resulting in phase-locked centers of ABL wind divergence and convergence that propagate westward with the TIWs.

With the availability of high resolution satellite wind and SST data, Chelton et al. (2001) were able to investigate in detail the dependency of the wind stress divergence and curl fields on the angle between the SST gradient vector and the wind stress. SST and wind stress fields were zonally high-pass filtered to remove the large-scale background variability with zonal wavelength longer than 20°. The anomalous wind stress divergence in the TIW region was found to be proportional to the downwind component of the SST anomaly gradient, while the anomalous wind stress curl was proportional to the anomalous cross wind component of the SST component. These robust relationships were found to persist throughout the period of strong TIW activity.

The phase relation between SST and latent heat fluxes were described by Liu et al. (2000). The latent heat flux was calculated from remotely obtained

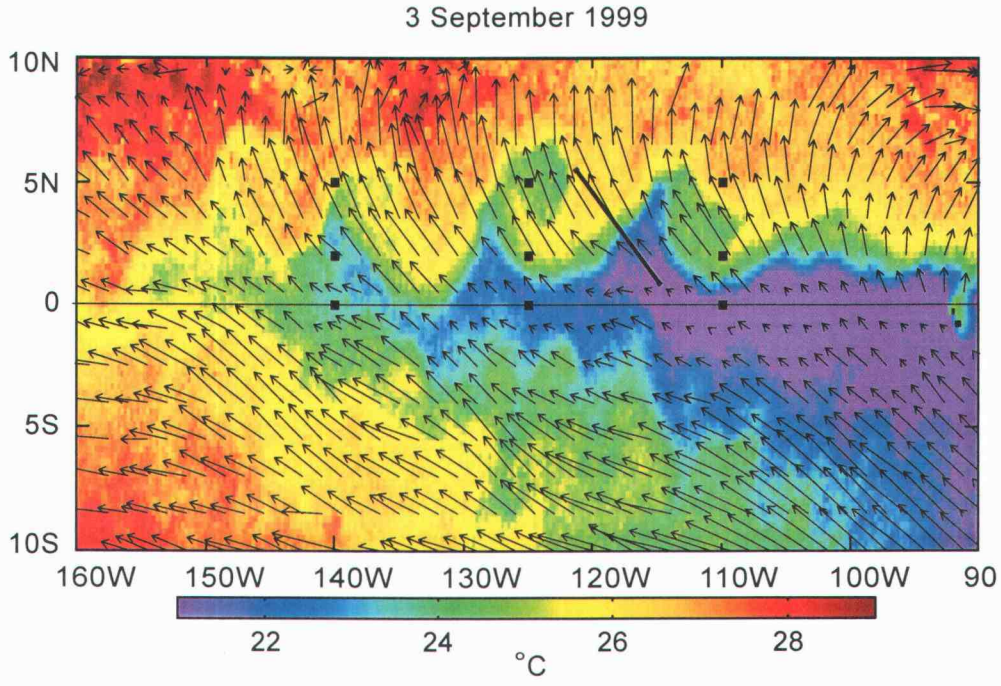

FIGURE 1.1 Three-day average map over the period 2-4 September 1999 showing sea surface temperature (color), and wind stress (vectors), and TAO mooring locations (squares). An idealized ABL column trajectory is indicated as diagonal bar.

SST, wind speed and integrated water vapor using the methodology developed by Liu (1988). They showed that latent heat flux is in phase with SST and wind speed, but the magnitude could not be determined with confidence due to the inaccuracy of the latent heat flux calculation on time periods shorter than 10 days (Liu et al. 1991).

The remote influence of TIW to the variability of the hydrological variables of integrated water vapor, cloud liquid water and precipitation was shown by Hashizume et al. (2001). The patterns of these variables north of 6°N are shifted

towards the west relative to the pattern of SST. Increased water vapor, liquid water and rain are found in regions of wind convergence.

The association of accelerating surface winds with cross strong SST gradients suggests the possibility of strong air-sea heat exchange. Zhang and McPhaden (1995) pointed out that as surface winds cross the SST front towards warmer water to the north of the cold-tongue, surface sensible heat and evaporation increase greatly. They estimated a change in latent heat flux of about 50 Wm^{-2} per 1 K change in SST. The reduction in solar radiation due to enhanced low-level cloudiness over the warm water was estimated by Deser et al. (1993) to be about 25 Wm^{-2}. A more detailed analysis of the latent and sensible heat fluxes in relation to the SST pattern can provide further insight into the mechanisms that modify ABL structure across the SST front.

In this study, estimates of surface sensible and latent heat fluxes are calculated from the surface and near-surface in situ measurements provided by the Tropical Ocean-Global Atmosphere (TOGA) Global Atmosphere Ocean (TAO) mooring array (McPhaden et al. 1998). Remotely sensed data are used to establish the relationship between SST and wind patterns and the TAO time series at nine mooring locations (140°W, 125°W, 110°W at 0°N, 2°N and 5°N). Through compositing, the in situ and remotely sensed observations of heat flux and wind stress can be *collectively* interpreted as a response to recurring TIW patterns of SST. Two compositing techniques are used to answer the following questions about the ABL response: (1) How does an idealized ABL air column respond when crossing the SST front near 2°N? and (2) What is the spatial and temporal relation between the responses at 2°N and 5°N for a typical wave cycle?

The data sets that were used for the analysis are summarized in Section 2, followed by explanations of the data processing issues, heat flux calculations and

compositing methods in Section 3. In Section 4, the results of the two compositing methods are presented separately while in Section 5 the compositing methods are combined to obtain a detailed picture in terms of magnitude and regional distribution of air-sea heat exchanges.

2 DATA DESCRIPTION

This study uses independent observations of SST, wind stress and surface meteorological variables from satellite and buoy platforms. The analysis benefits from the individual advantages of the observational platforms. The in situ measurements from the TAO mooring array provide the crucial surface and near-surface measurements of meteorological variables that are needed to calculate a reliable estimate of sensible and latent heat flux. The satellite data allow the placement of the buoy point measurements in their spatial context relative to the TIW perturbations of SST and wind (Fig. 2.1).

The availability of wind stress data from the QuikSCAT instrument during the TIW 1999-2000 season restricts the analyzed time period. We have chosen the 28 July 1999 to 27 January 2000 time period for the analysis.

The buoy measurements from the TAO mooring array provide the in situ data set consisting of SST at 1 m depth, air temperature and relative humidity at 3 m height and the wind speed and direction at 4 m height. We use daily averaged data to resolve the atmospheric response to the oceanic forcing by TIWs which have periods of 20 to 40 days. Since this investigation is focused on the ABL response to SST perturbations resulting from TIWs, nine buoy locations along 0° N, 2° N and 5° N at 140° W, 125° W and 110° W were chosen, covering the region of high TIW variability (see Figs. 1.1, 2.1a, black squares indicate buoy locations).

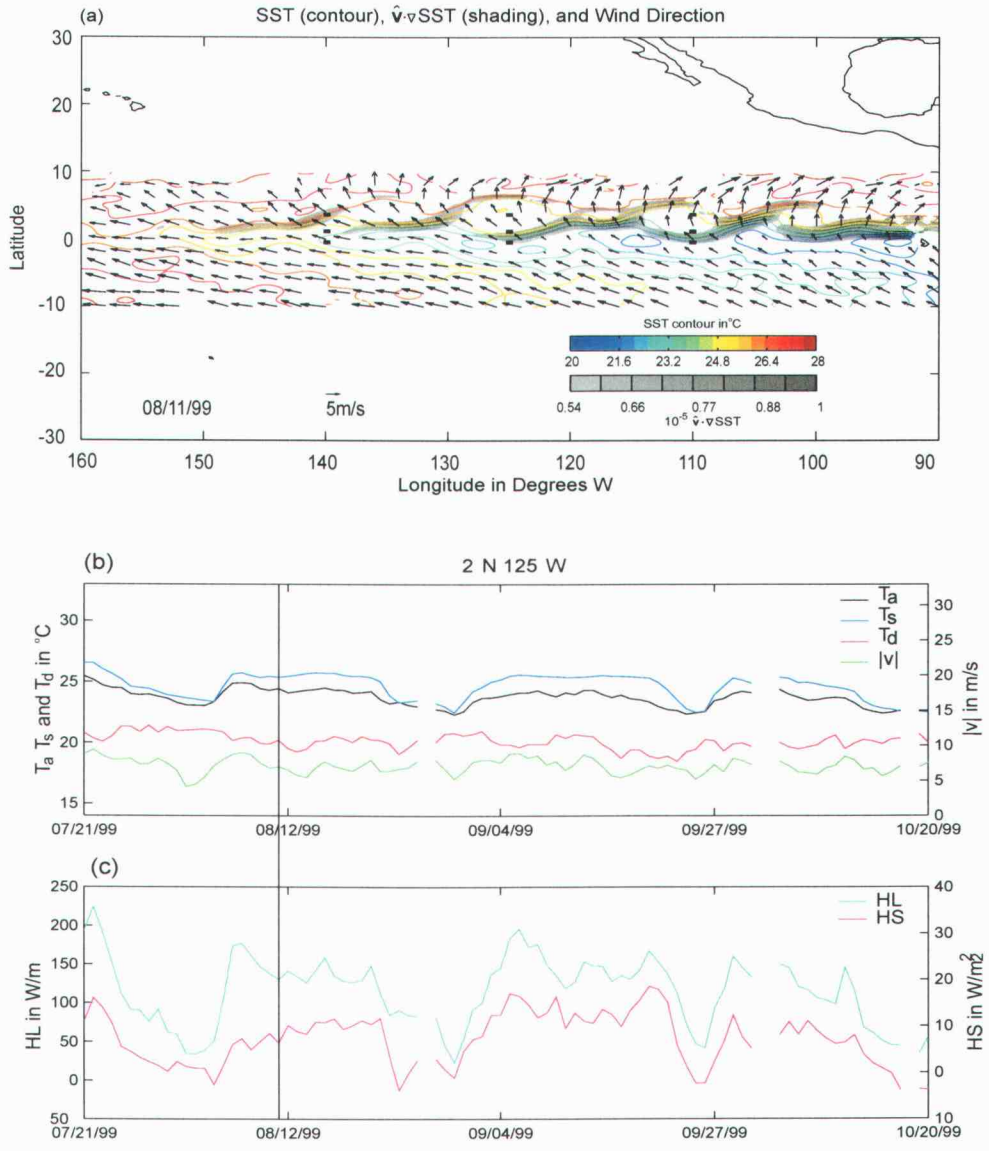

FIGURE 2.1 (a) Three-day average map from 8 August 1999 showing TMI SST as contours, QuikSCAT wind vectors, calculated downwind component of ∇ SST shaded and TAO buoy locations as squares; (b) time series of daily average air, sea and dew point temperature and wind speed magnitude from the TAO mooring at 2°N, 125°W. Vertical bar indicates the corresponding date of the map shown in (a); and (c) time series of corresponding sensible and latent heat flux.

Detailed spatial information is obtained from the combined use of observed SST and wind data sets from satellites. The SST data are provided by the TRMM Microwave Imager (TMI) onboard the Tropical Rainfall Measuring Mission (TRMM) satellite (Kummerow et al. 1998). These data were analysed to provide three-day mean fields with a spatial resolution of 46 km. The TMI SST measurements are based on the 10.7 GHz brightness temperature which has a very small atmospheric contribution, except for heavy rain measurements that are flagged and removed. The SST measurement accuracy has been shown to be better than 0.5 °C for the region of interest here (Chelton et al. 2001).

Surface wind stress was measured by the SeaWinds scatterometer onboard the QuikSCAT satellite. The 6-month QuikSCAT data record analyzed here begins on 28 July 1999. The instrument provides equivalent neutral-stability vector wind estimates with a 25-km resolution over a single 1600-km swath which is then interpolated and smoothed to obtain daily maps of overlapping three-day averages on a 0.25° spatial grid.

3 METHODOLOGY

The buoy time series of meteorological variables suggest a strong influence of TIWs on atmospheric boundary layer processes in the region of interest (Fig. 2.1b,c). Sensible and latent heat fluxes are inhibited during periods when the mooring is located in the relatively cool water of the TIW cusps. A sharp increase in SST indicates the passage of the TIW-induced SST front where sensible and latent heat fluxes increase rapidly. During the warm phase with relatively high SST, the fluxes of sensible and latent heat remain high but decrease rapidly with passage of the cold front of the TIW-induced SST wave. It is apparent that the regimes over the cold and warm water are significantly different and that the ABL response to the TIW disturbances is crucial to understanding the boundary layer physics of the region. Time series from the sparse distribution of the TAO moorings do not resolve the spatial structure of TIWs. To interpret the buoy time series in the context of the propagating TIWs, it is necessary to transform the contineous temporal information of the mooring time series to more relevant spatial and phase information related to the propagating TIWs with the help of satellite data. The simultaneous usage of satellite and in situ measurements and the transformation from time to space/phase allows the interpretation of sparse buoy data with respect to the propagating TIW signals. This interchange of time and space is described Section 3.1, and the transformation from time to phase is discussed in Section 3.2.

We study the ABL response using two different compositing methods – Lagrangian compositing along trajectories and and Eulerian compositing relative to the TIW phase. For the Lagrangian trajectory method, the ABL response is investigated following an idealized ABL air column propagating across the nothern equatorial SST front from cold to warm water. As the time series of meteorolog-

ical variables indicate (Fig. 2.1b,c), the buoys at 2°N are located in a region with high SST variability of 3-4°C associated with TIWs. Depending on the phase of the TIW, the buoys can be located in warm or cold water or in the transitional frontal region. The wind vectors and the SST pattern can be used to construct idealized ABL trajectories and to composite sensible and latent heat fluxes and other meteorological variables depending on the measurement's location relative to the position of the SST front.

For the Eulerian wave composite, the regional ABL response to the spatial pattern of TIW-induced SST variability is of interest. From this perspective, both the SST pattern and the ABL response show a wavelike behavior. The recurring characteristics of the wavelike atmospheric response can be composited using the phase information of the waves inferred from the SST field.

3.1 Trajectory-compositing

This compositing method transforms the independent variable 'time' of the buoy point measurements into 'space' using satellite maps of SST and wind. For this analysis the distance between the buoy and the SST-front along an air parcel trajectory across the front is of interest (see Fig. 3.1). For each measurement in the buoy time series, the wind field defines trajectories connecting the buoys with the upstream front. The time required for an air parcel to cross the SST front is much shorter than the time scale of TIW change at a point in space, because the phase propagation of the TIWs is about $0.5 \mathrm{ms}^{-1}$ while the wind speed is on the order of $10 \mathrm{ms}^{-1}$. Each buoy location can be associated with a distance along the trajectory to the SST front. In this manner the time series are enhanced by relating the spatial information from the satellite maps to the time series.

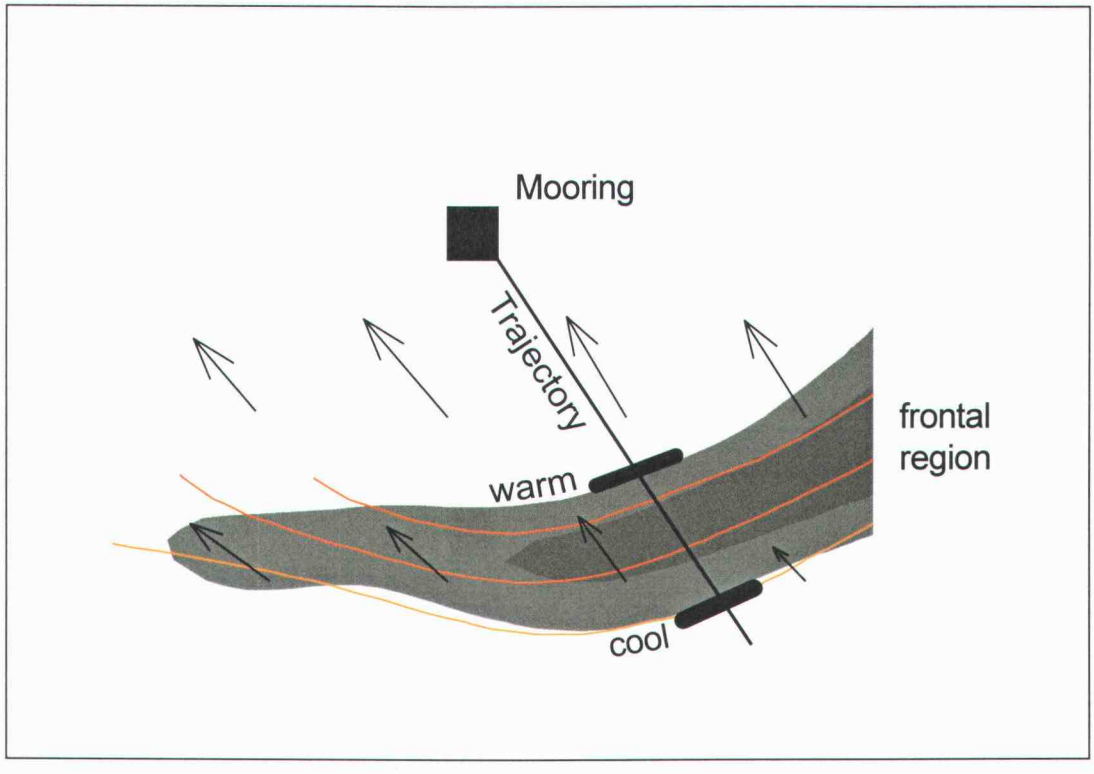

FIGURE 3.1 Typical structure of mooring and SST front, where the mooring is located downstream from the front

This compositing method requires a definition of the boundaries of the frontal region from which the distance from the buoys can be measured. We chose the magnitude of the downwind component of the SST gradient, i.e., $\hat{v} \cdot \nabla T$, where $\hat{v}$ is the unit wind vector and T the SST, to identify the region of potentially strong air-sea interaction along the SST front. Areas where $\hat{v} \cdot \nabla T$ exceeds 5.4×10^{-6}K/m is considered as part of the frontal region with frontal boundaries of $\hat{v} \cdot \nabla T = 5.4 \times 10^{-6}$K/m.

The quantity $\hat{v} \cdot \nabla T$ was calculated from QuikSCAT vector wind and TMI SST. The 3-day mean QuikSCAT wind field defines the idealized trajectory and it determines whether the front is located in upstream or downstream direction from the mooring location. The trajectory containing the buoy location for a given 3-day period intersects the frontal region at both the warm and the cold side of the front. Each buoy observation in the time series was assigned a distance to an SST frontal boundary along the trajectory (see Fig. 3.1). For rare cases when an upstream and a downstream frontal region were present, only the upstream frontal region was chosen. To account for different widths and to avoid smearing the edges of the frontal region, *two* distances were measured: (1) the distance to the warm side and (2) to the cold side of the front. Distances were either taken positive for measurements in the upstream direction or negative in the downstream wind direction. The data are divided into three regions: (1) upstream from the front, (2) in the front and (3) downstream from the front. For the first and last case, the data are binned as a function of the distance in km to the closest frontal boundary (i.e., the warm side in Region 1 and the cold side in Region 3). For the second region where the buoy is located within the front, the distance to either side is normalized by the width of the front and is interpolated in relative units (see Fig. 4.1). The results of this method will be presented in Section 4.1.

3.2 Wave-compositing

The spatial structure in the SST field in the satellite maps provides information about the phase of the TIWs. We use complex empirical orthogonal functions (CEOFs) to provide an objective means of determining the phase of TIW vari-

ability (Barnett 1983). The CEOF analysis allows a phase angle to be assigned to each TAO measurement time. Then, compositing is performed by averaging TAO measurements having similar phase angles. The resulting data set provides boundary layer measurements as a function of TIW phase angle. By using the wave phase angles at 2°N as a reference, the structure that is coherent with the strongest TIW activities at 2°N is revealed by compositing buoy and satellite measurements at all latitudes to obtain phase-latitude maps. These maps can be used to infer the spatial and temporal response of the ABL to TIW disturbances (Fig. 4.2).

The phase information for this compositing method is based on a CEOF analysis of TMI SST anomalies. The CEOF analysis is an extension of classical EOF analysis to describe travelling wave patterns in a single complex mode (Horel 1984). This is obtained by adding the Hilbert transform

$$y_H(t) = \frac{1}{\pi}\int_{-\infty}^{\infty}\frac{y(t')}{t-t'}dt' \tag{3.1}$$

$$= h(t) * y(t) \tag{3.2}$$

$$h(t) \equiv \frac{1}{\pi t} \tag{3.3}$$

to the original time series at each location x_m to form the complex analytical signal

$$z(x_m, t) = y(x_m, t) + iy_H(x_m, t) \tag{3.4}$$

For practical considerations, the convolution (3.2), which is defined for a continuous, infinite process $y(t)$, is approximated by a discrete convolution

$$\hat{y}_H(t_n) = \sum_{m=-M}^{M} y(t_n - m\Delta t)\hat{h}(m\Delta t) \tag{3.5}$$

where Δt is the discrete sample interval, $M\Delta t$ is the half span of the convolution filter and $\hat{h}(m\Delta t)$ is the filter. Oppenheimer and Schafer (1975) suggest the simple but adequate filter

$$\hat{h}(m\Delta t) = \begin{cases} \frac{2}{\pi m}\sin^2(\pi m\Delta t/2) & \text{if } m \neq 0 \\ 0 & \text{if } m = 0 \end{cases} \tag{3.6}$$

The filter function (3.6) provides the desired properties of approximate unit amplitude response and $\pi/2$ phase shift. To reduce the effect of "ripples" in the Hilbert transform within $M\Delta t$ of the edges of the data record, M is commonly restricted to relatively small values (in this analysis $M = 7$) and data values within $M\Delta t$ of the beginning and end of the data record are eliminated.

The CEOF decomposition of the analytical signal $z(x_m, t)$ at location x_m is

$$z(x_m, t) = \sum_{k=1}^{K} a_k(t) F_k(x_m) \tag{3.7}$$

with the orthonormality condition for the basis vectors $F_k(x_m)$

$$\sum_{m=1}^{M} F_j(x_m) F_k(x_m) = \delta_{jk} \qquad \delta_{jk} = \begin{cases} 1 & \text{if } j = k \\ 0 & \text{otherwise} \end{cases} \tag{3.8}$$

The complex mode k CEOF $F_k(x_m)$ and its corresponding complex amplitude time series $a_k(t)$ can be expressed in polar coordinates. The CEOF expansion in terms of amplitude and phase is then

$$z(x_m, t) = \sum_{k=1}^{K} A_k^a(t) e^{i\phi_k^a(t)} A_k^F(x_m) e^{i\phi_k^F(x_m)} \tag{3.9}$$

where

$$A_k^F(x_m) = [F_k^*(x_m) F_k(x_m)]^{1/2} \tag{3.10}$$

$$\phi_k^F(x_m) = \tan^{-1}\left(\frac{\mathrm{Im}[F_k(x_m)]}{\mathrm{Re}[F_k(x_m)]}\right) \tag{3.11}$$

$$A_k^a(t) = [a_k^*(t) a_k(t)]^{1/2} \tag{3.12}$$

$$\phi_k^a(t) = \tan^{-1}\left(\frac{\mathrm{Im}[a_k(t)]}{\mathrm{Re}[a_k(t)]}\right) \tag{3.13}$$

During the period of interest, the pattern of propagating disturbances associated with TIWs is well represented by the first mode. The analysis provides the spatial phase $\phi_1^F(x_m)$ and temporal phase $\phi_1^a(t)$ for this mode which can be used as described by (REFS) to calculate phase speed estimates in the time-longitude domain,

$$c_p(x_m, t) = \frac{d\phi_1^a(t)/dt}{d\phi_1^F(x_m)/dx} \tag{3.14}$$

where ϕ_1^F is the spatial phase of the first CEOF mode calculated from TMI SST data along the 2°N parallel from 90° to 160° longitude and from 0° to 6° latitude. These phase speed estimates, when overlaid on the Hovmöller diagram of SST anomalies (Fig. 3.2), define the phase propagation. Any chosen phase angle at the beginning of the data record or along 103°W, i.e the lower and right hand sides in Fig. 3.2, can be traced throughout the Hovmöller diagram along contours of constant phase angle. As shown in Fig. 3.2, these phase lines for the first CEOF mode follow very closely the TIW propagation in the full anomaly field (Fig. 3.2b) constructed from TMI SST. The SST anomalies in the reconstructed SST-field from mode 1 (Fig. 3.2c) are clearly an important part of the total TIW SST variability. This mode explains 26 % of the total variance. Inferring the phase state of the wave from the mode-1 CEOF, the TAO mooring time series can be resampled as a function of phase angle (see 4.2).

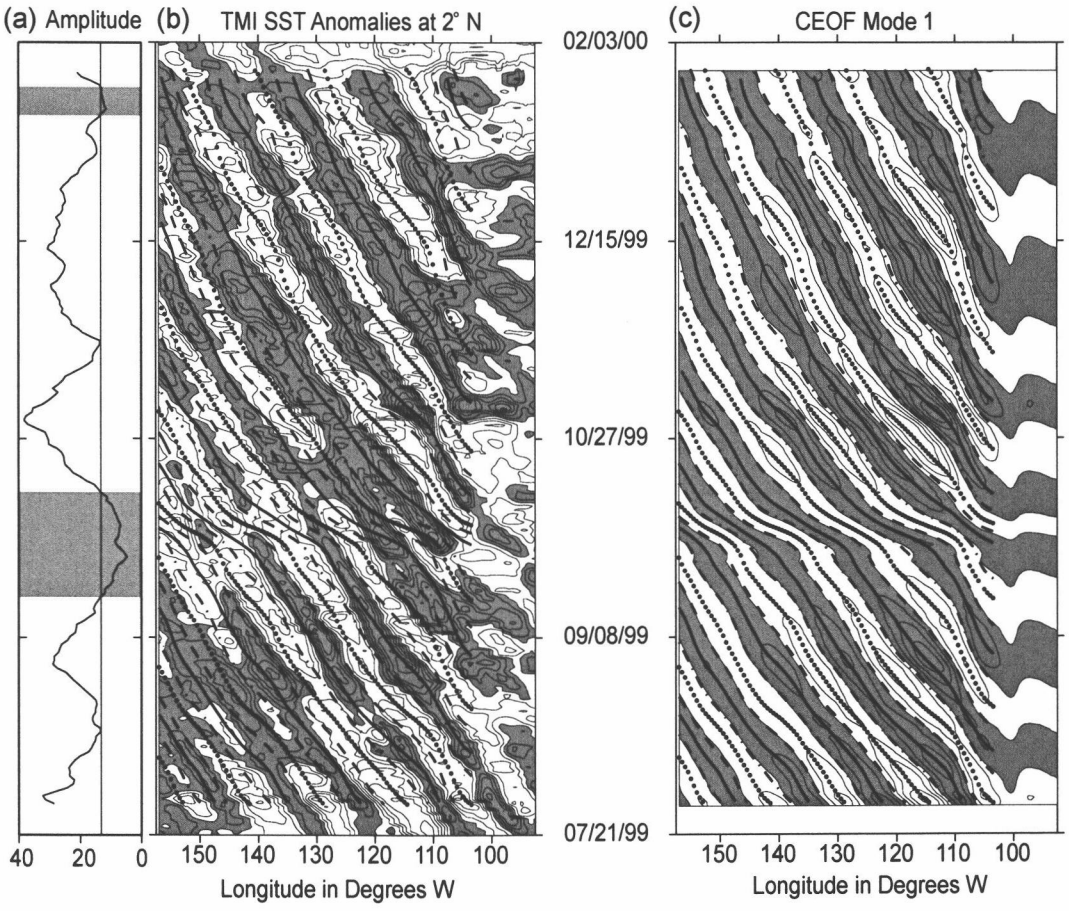

FIGURE 3.2 (a) Mode 1 amplitude time series with cutoff value shaded. (b) Hovmöller diagram of TMI SST anomalies at 2°N. Gray (white) shaded areas correspond to negative (positive) anomalies. Contour interval is 0.5°C. (c) Hovmöller diagram of reconstructed mode 1 SST anomalies at 2°N with superimposed phase lines. The lines superimposed on panel b and c represent 0° (black), 90° (dashed), 180° (dotted) and 270° (dash-dotted) phase angle from the dominant CEOF shown in panel (c).

3.3 Heat flux calculations

The Version 2.6 COARE algorithm (Grachev and Fairall 1997; Grachev et al. 2000) is applied to the TAO in situ measurements to calculate the sensible and latent heat fluxes for the period from 28 July 1999 to 27 January 2000. We have included the cool skin effect, but not the subsurface warm layer physics (Fairall et al. 1996) since the lack of radiation and precipitation measurements makes the calculation of warm layer effects a practical impossibility. We believe, however, that the potential underestimation of the fluxes in the TIW region due to lack of warm layer effects is relatively small and that inclusion of this effect would not significantly alter the conclusion of this study. In the low wind stress region over the cold tongue, precipitation is light and the solar energy is probably distributed over a relatively thick oceanic layer and would therefore have little effect on the SST. Over the warm water, strong wind acts to distribute any accumulation of heat through enhanced vertical mixing of near surface water with deeper water and tends to destroy the warm surface layer. Weak wind stress is found only in the weakly stable boundary layer regime over the cold water. The wind stress increases rapidly across the SST front.

The error in the heat fluxes due to the neglect of warm layer effects is estimated by heat flux calculation at 0°N 110°W where a 90-day data record of shortwave radiation is available. The sensible heat flux was found to be underestimated by less than 0.5 Wm^{-2}, while the root mean square error in latent heat flux was about 1.2 Wm^{-2} when the shortwave radiation is omitted. These values represent 3.3% and 1.0% of the total change of 15 Wm^{-2} and 120 Wm^{-2} of sensible and latent heat fluxes across the front, respectively. The error estimate is insensitive to changes in the cloud parameterization which was neglected for the sensible and latent heat fluxes calculated in this analysis.

The longwave radiation flux needed for the cool skin calculation is obtained using the bulk formula of Berliand (1952). This approximation is a simple balance between an estimate of the upward cloud-free net loss of longwave radiation at the ocean surface determined by the air and sea temperatures and the downward radiation flux due to clouds and moisture. The net flux for infrared radiation is given by:

$$F_l \approx \epsilon\sigma T_a^4 \cdot (p - q\sqrt{e}) + 4\epsilon\sigma T_a^3 (T_s - T_a) \tag{3.15}$$

where T_a and T_s are the daily mean air and sea surface temperatures, e is the water vapor pressure (in hPa), ϵ is the emissivity of water (= 0.97) and σ is the Stefan-Boltzmann constant. According to Berliand (1952), the coefficients p and q are constants equal to 0.39 and 0.05, respectively.

4 RESULTS

The results are presented for the two compositing methods separately. The Lagrangian trajectory-compositing in Section 4.1 describes an ABL air column as it is advected across the SST gradient. The Eulerian phase-compositing in Section 4.2 determines the regional ABL responses to SST distributions. The complementary aspects of the two compositing methods are discussed in Section 5.

4.1 Trajectory-compositing

If the wind direction does not change rapidly with height, the prevailing southeasterly winds at the surface may be used to determine the trajectory of an idealized ABL air column as it is advected from the cool to the warm side of the SST front. In this case, the graphs shown in Fig. 4.1 may be regarded as the near-surface meteorological conditions and heat fluxes along the ABL trajectory from southeast (cool side) to northwest (warm side). For an ABL air column traveling across the SST gradient, the SST field can be regarded as stationary, because wind speed of more than 5 ms^{-1} is more than 10 times larger than the TIW phase speed of $\sim$ 0.5 ms^{-1}. The mean standard errors for the presented properties are included in Fig. 4.1.

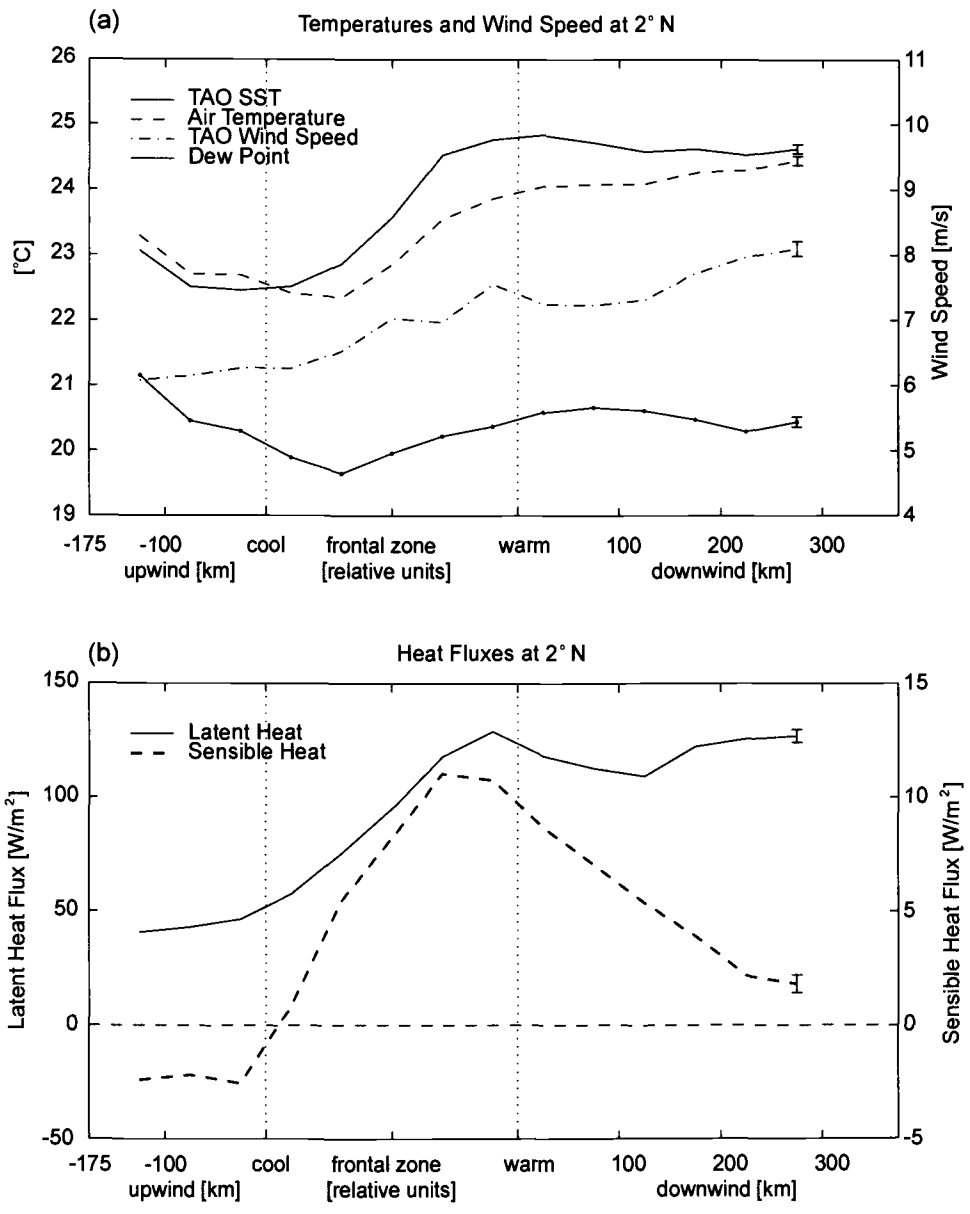

FIGURE 4.1 (a) Binned TAO SST, TAO air temperature, TAO wind speed and dew point temperature as function of distance relative to the frontal zone; (b) same as (a) for binned latent and sensible heat flux. Vertical bars represent mean standard errors.

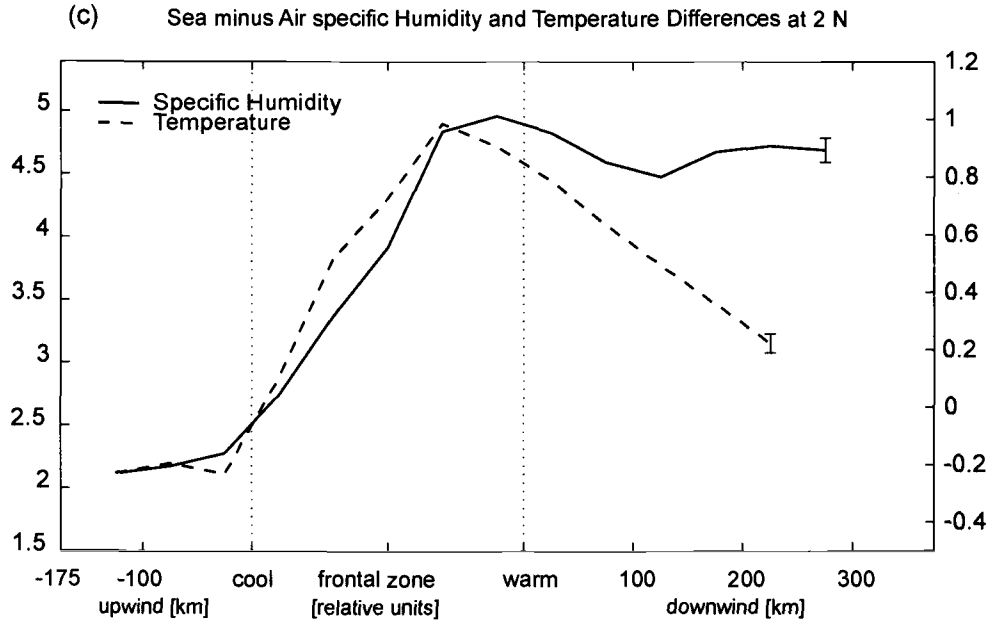

FIGURE 4.1, (continued) (c) The same as (a) for binned sea surface minus air temperature and sea surface minus air specific humidity. Vertical bars represent mean standard errors.

Following an ABL air column from cold to warm water across the SST gradient, it is apparent that sensible and latent heat fluxes are inhibited on the cold side of the front. Sensible heat flux is slightly negative (-2 Wm^{-2}) and latent heat flux is less than 50 Wm^{-2} (Fig. 4.1b). The TAO measurements of SST are about 22.5 °C on the cold side of the front (Fig. 4.1a). The latent heat flux and the associated sea surface minus air specific humidity is small, while the sensible heat flux is negative corresponding to the sea surface minus air temperature differences which is slightly negative (Fig. 4.1c). The TAO measurements of wind speed on the cold side are $\sim$ 5.5 ms^{-1} (Fig. 4.1a).

Entering the frontal zone, sensible and latent heat fluxes, SST, wind speed and sea surface minus air specific humidity and temperature differences increase significantly. The maxima of these quantities are found on the warm side of the frontal region. The maximum of sensible heat flux is 11 Wm^{-2}, whereas the latent heat flux reaches a maximum of about 120 Wm^{-2} (Fig. 4.1b). The wind speed increases to about 7.5 ms^{-1} (Fig. 4.1a).

North of the frontal zone, over the warmer water, the responses of sensible and latent heat fluxes are remarkably different. While sensible heat flux decreases to values of about 2 Wm^{-2}, latent heat flux remains at a large value of more than 110 Wm^{-2} (Fig. 4.1b). The behavior of the sea minus air specific humidity and temperature differences are consistent with the latent and sensible heat fluxes, respectively. The wind speed remains more or less constant at 7.5 ms^{-1} (Fig. 4.1a).

It is apparent that sensible and latent heat fluxes increase over the strong SST gradient and large values of latent heat fluxes are found over the warm water. The increase in surface wind speed in the region of enhanced sensible and latent heat fluxes is consistent with the ABL momentum mixing hypothesis. The associated cold air advection is responsible for the location of the maxima heat fluxes where the SST gradient increases (Fig. 4.1a). The changes of sensible and latent heat fluxes along the trajectory are very similar to the changes of the sea-minus-air temperature and specific humidity differences, respectively (Fig. 4.1c).

4.2 Wave-compositing

The spatial and temporal structure of the ABL response to TIWs can be characterized alternatively as a function of wave phase angle. As described in

Sec. 3.2, the space-time phase angle at the buoy locations can be objectively determined from the CEOF analysis at all times, and the heat fluxes can be composited for measurements with similar phase angles. Although only 26 % of the variance is explained by mode 1, Fig. 3.2 shows that the features of the TIW amplitude and phase propagation that are most important for the compositing are captured by mode 1; higher modes primarily describe localized strengthening and weakening of the anomalies. The calculated phase lines follow the propagation of positive (dotted lines) and negative (black lines) anomalies remarkably well (Fig. 3.2b), especially in regions where the amplitude of the CEOF time series (Fig. 3.2a) is large. The phase lines are less useful in transitional states of the TIW field, for example in the early part of Oct. 1999 (Fig. 3.2b) where the mode 1 amplitude time series is small (Fig. 3.2a). The amplitude time series can therefore be used as an indicator of how well mode 1 phase lines represent the propagation of the anomalies. We have chosen an amplitude threshold of about 30% of the maximum amplitude to identify time periods when mode 1 is not representative of the TIW phase propagation and TIW amplitude. These time periods (shaded in Fig. 3.2a) were excluded from the analysis presented below. The analysis is insensitive to the explicit choice of the threshold. Eight phase angles have been chosen to composite sensible and latent heat flux, specific humidity and temperature time series as a function of phase state. The results are shown in Figs. 4.2 and 4.2.

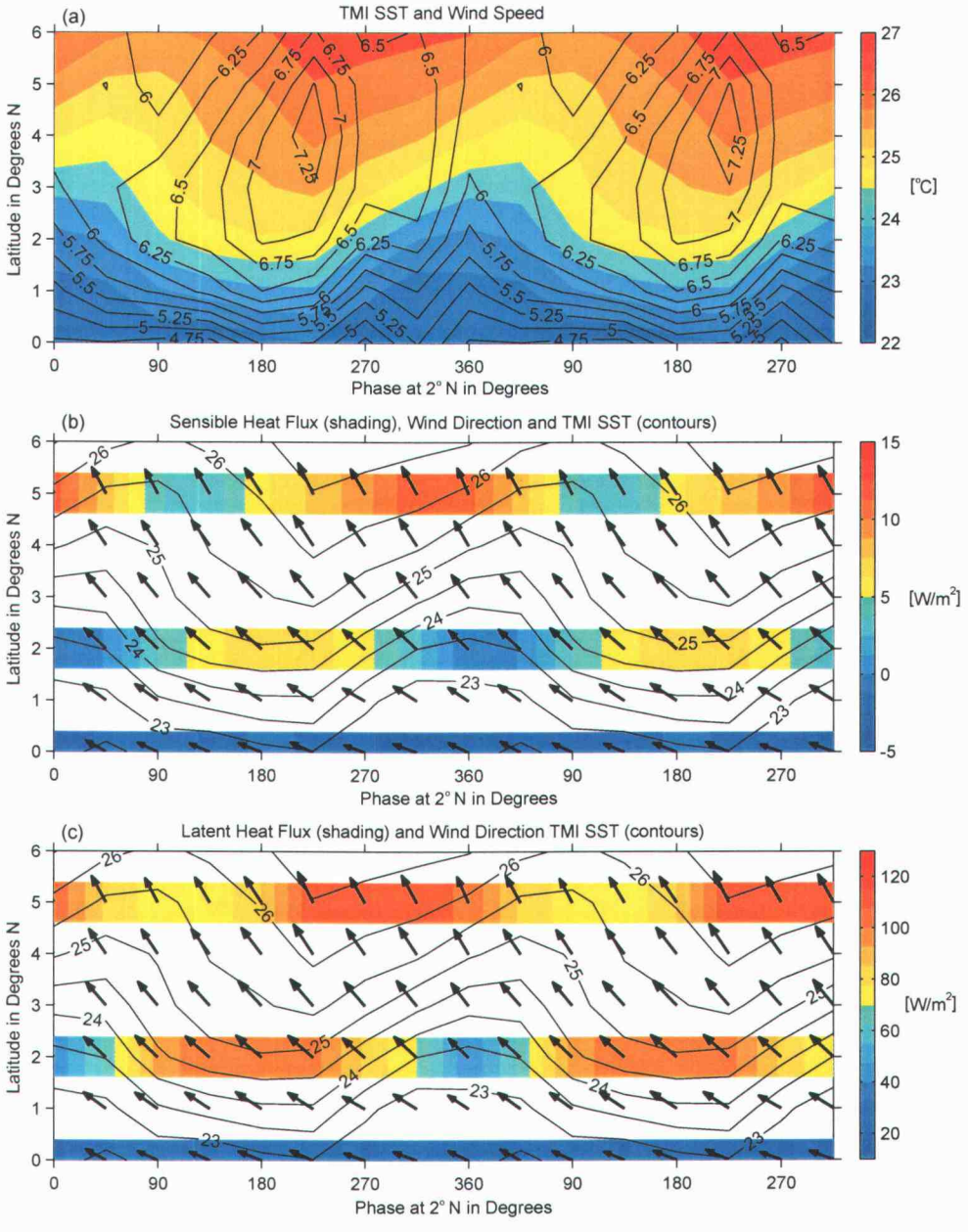

FIGURE 4.2 Phase-latitude maps of (a) TMI SST (shading) and wind speed, (b) sensible heat flux (shading), wind direction and TMI SST (contours), and (c) latent heat flux (shading), wind direction and TMI SST (contours).

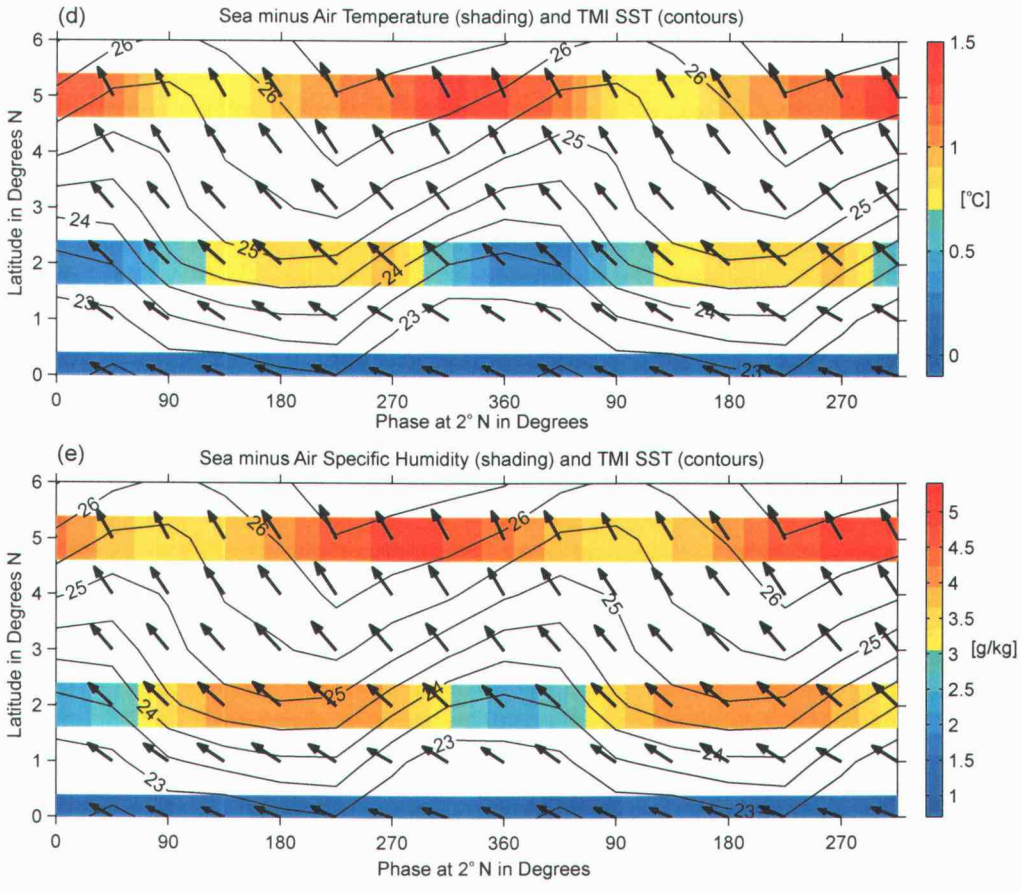

FIGURE 4.2, (continued) (d) sea surface minus air (shading), wind direction and TMI SST (contours), (e) sea-minus-air specific humidity (shading), wind direction and TMI SST (contours).

All time series are composited as a function of the wave phase angle at 2°N. The latitude of 2°N was chosen because the SST signature of TIW disturbances are most energetic at this latitude (Chelton et al. 2000). The interpolated and smoothed QuikSCAT wind speed and TMI SST measurements are displayed here on a one degree grid which enables the presentation of longitude-phase maps of TMI SST and wind speed (Fig. 4.2a), demonstrating the general characteristic

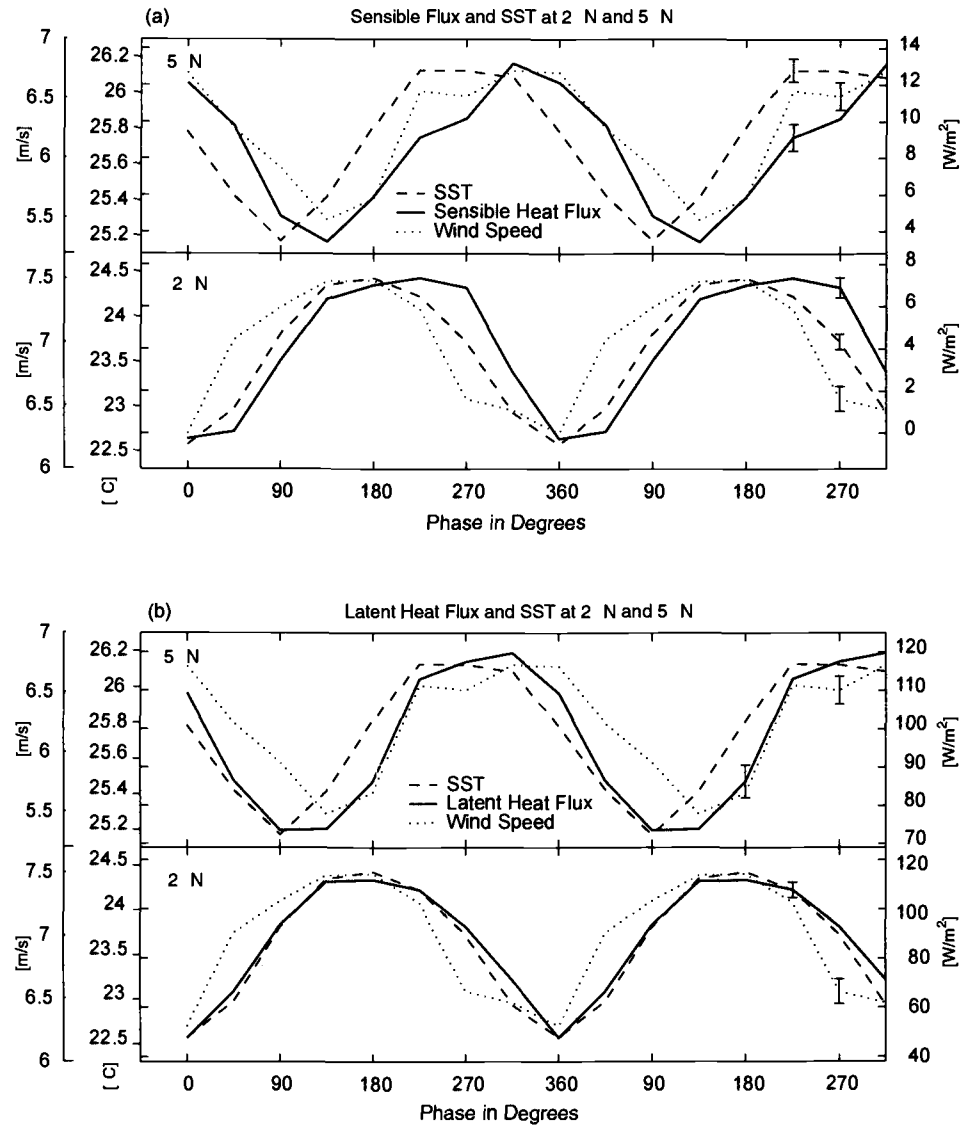

FIGURE 4.3 (a) Latent heat flux and SST: top panel at 5°N, bottom panel at 2°N. (b) Sensible heat flux and SST: top panel at 5° N, bottom panel at 2° N. Vertical bars represent mean standard errors

of the SST and the wind patterns associated with TIWs. The longitude-phase structure of the composited TIW disturbance is shown in Fig. 4.2, while the presentation as line plots in Fig. 4.2 better reveal the magnitude and phase shift of the processes. The phase cycle is repeated twice for clarity and vertical bars represent the standard error. The eastward tilting of the cold cusps with increasing latitude can be seen in Figs. 4.2a and 4.2 which was also seen in the snapshots of SST in Fig. 1.1. It is apparent from the composited wind vectors (Fig. 4.2b) that the wind direction is not strongly affected by the SST perturbations associated with TIWs. However, the wind speed varies by $\sim$ 1 ms^{-1} in response to the underlying SST field (Figs. 4.2a, 4.2) at a given latitude.

A striking feature in Fig. 4.2b and Fig. 4.2a is the eastward shift of sensible heat flux at 2°N and especially at 5°N relative to the pattern of TMI SST. This shift is most clearly seen in Fig. 4.2 but it is also apparent in Fig. 4.2. The coupling of sensible heat flux to regions of strong SST gradients results in a southwest-to-northeast phase-shift between the two latitudes that is associated with the tilting of the SST phase lines with increasing latitude. The relatively broad maximum of sensible heat flux at 2°N at phase angles between 135°and 270° may be related to the proximity of the front to the mooring location at all wave angles of the warm phase which would cause ABL adjustments and air-sea interactions. The maximum of sensible heat flux is located in a region of strong SST gradient at a phase angle of 225°.

The patterns of latent heat flux in Fig. 4.2c and 4.2b show the eastward shift only at 5°N, not at 2°N. As seen in Fig. 4.2b the latent heat flux response has a broad maximum and a sharp cusp-shaped minimum at 2°N. The response is symmetric about the maximum. At first glance, this appears to be inconsistent with the result from Fig. 4.1 where we found a sharp increase in latent heat flux

across the strong SST gradient and an almost constant plateau value over the warm water downstream of the frontal boundary. It appears however that the CEOF compositing method has difficulties resolving the details of the pattern of latent heat flux and SST. This is likely due to the fact that each realization of the TIW is different. The CEOF composite method thus results in smoothing. The composite flux and SST patterns which are expected to be similar to those seen in Fig. 4.1 are smoothed near the transition from large SST gradient in the frontal zone to the plateau values over the warm water to the north. This smoothing of the gradients on either side of the front (from cold to warm and from warm to cold) could account for the observed shape of latent heat flux.

The patterns of sensible and latent heat flux are closely related to the pattern of sea-minus-air temperature (Fig. 4.2d) and sea-minus-air specific humidity (Fig. 4.2e), respectively. The humidity difference pattern is shifted to the east at 5°N, but not at 2°N, whereas the pattern of the temperature difference is clearly shifted at both latitudes with a double peak structure at 2°N in the warm pool.

5 DISCUSSION AND CONCLUSIONS

The two compositing methods presented in this study allow a detailed description of near surface boundary layer conditions across the perturbed SST front. It has been shown that the boundary layer response to oceanic forcing by the SST is shifted eastward relative to the pattern of SST. The spatial shift is larger at 5°N than at 2°N. The enhancement of sensible heat flux across the front is a much larger fraction of its background values on either side of the front than is the enhancement of latent heat flux. On the larger scale, relatively warm water in TIW disturbances is associated with relatively large sensible and latent heat fluxes. Over relatively cool water, the fluxes are smaller. However, temperature advection appears to have an important effect on the ABL heat budget and shifts the sensible heat flux pattern toward the east relative to the SST anomalies.

Sweet et al. (1981) hypothesized that the acceleration of boundary layer air across an SST front can be caused by enhanced downward mixing of momentum in the unstable boundary layer regime. Hayes et al. (1989) proposed this mechanism to explain the observed wind patterns in association with TIW-induced SST perturbations. The enhanced momentum mixing is expected to be accompanied by increased sensible and latent heat fluxes. The boundary layer may be out of equilibrium if the change of temperature at the surface is rapid. The adjustment time scale may be larger downstream from the frontal zone than within the frontal zone and the ABL properties may adjust more slowly to the equilibrium values.

By combining the results of the two compositing methods, a detailed picture of air-sea interaction can be obtained in terms of magnitude and distribution of surface sensible and latent heat flux responses to TIWs. It is clear that the atmospheric response provides a negative feedback to the TIW SST anomalies in this region. Latent and sensible heat fluxes tend to cool the positive and warm

the negative SST anomalies. The latent heat flux anomalies of about 40 Wm^{-2} are the primary contributor to the cooling/warming of the SST anomalies. This is consistent with the estimate of 50 Wm^{-2} per 1 K SST change obtained by Zhang and McPhaden (1995) from much more limited dataset. Distributing the 40 Wm^{-2} latent heat flux over a layer of about 50 m depth yields an instantaneous heating rate is 1.6×10^{-2} K/day. For a typical TIW periodicity of 30 days, the temperature change due to latent heat flux would be about 0.5°C. In addition, the enhanced vertical mixing over the warmer water generates increased low-level cloudiness that reduces the solar insolation that reaches the sea surface (Deser et al. 1993). If the compensating longwave effect of the clouds is taken into account, the cooling effect from the increased cloudiness may be as large as ~ 0.6 °C per month (Deser et al. 1993).

The comparison of the humidity and temperature differences across the SST front and over the warm water to the north suggests that the temperature structure of the boundary layer adjusts more rapidly than the moisture structure across the SST-front. A similar difference of the adjustment times of the humidity and temperature field was also observed by Friehe et al. (1991) during the FASINEX experiment in the western North Atlantic.

The results obtained here are consistent with the ABL momentum mixing hypothesis and can be seen as complementing results to prior work. The hypothesis explains not only the wind pattern but also predicts that the patterns of sensible and latent heat flux are shifted relative to the frontal pattern of SST.

The ABL momentum mixing hypothesis appears to successfully explain the surface wind acceleration in the presence of a low-level jet from which momentum can be mixed downward. Based on surface observations alone, however, it is not possible to infer with certainty that the increase in the speed of the low level

wind is solely due to this mechanism. It is possible that a low level pressure adjustment (Hashizume 2001, Wai and Stage 1989; Lindzen and Nigam 1987) may also be important. In addition, the model study by Wai and Stage (1989) suggests that a low-level thermally direct circulation in the cross frontal direction may be responsible for a significant amount of the surface wind acceleration near the surface. The lower branch of a secondary circulation caused by pressure adjustments to the SST distribution across the frontal region distribution is in the same direction as the mean wind from cold to warm water and would thus tend to accelerate the near-surface wind. The upper branch of the circulation would oppose the mean flow and decelerate the flow aloft. The wind shear in the boundary layer would be reduced. The resulting wind profiles would tend to be similar to the profiles expected for the ABL momentum mixing hypothesis. Although the calculations by Wai and Stage (1989) show that the pressure term is most important for the acceleration in the lower level, the ABL momentum mixing hypothesis might still play an important role, and both mechanisms might be needed to explain ABL adjustments across SST gradients.

To distinguish the contributions of secondary circulation and vertical momentum mixing, detailed vertical profiles of boundary layer properties across the SST-front will be needed. Available radiosonde measurements (e.g., Liu et al. 2000) are not sufficient to allow budget calculations to sort out the relative importance of the pressure gradient versus the turbulent flux convergence. Future work will need to focus on investigation of the vertical structure of the boundary layer in order to distinguish between the various mechanisms. Multiple, synoptic, airborne measurements at different times of the day in conjunction with satellite observations would allow an extension of horizontal maps into vertical 2-dimensional or even 3-dimensional analyses of boundary layer structure and

heat, moisture and momentum budgets. These analyses should be accompanied by further modeling studies in the equatorial zone.

BIBLIOGRAPHY

Barnett, T. P.,1983: Interaction of the monsoon and Pacific trade wind system at interannual time scales. Part I: the equatorial zone. *Mon. Wea. Rev.*, *111*, 756-773.

Berliand, M. E., and T. G. Berliand, 1952: Determining the net long-wave radiation of the Earth with consideration of the effect of cloudiness. *Isv. Akad. Nauk. SSSR Ser. Geofiz, 1.*

Bond, N. A., 1992: Observations of planetary boundary-layer structure in the eastern equatorial Pacific, *J. Climate*, *5*, 699-706.

Chelton, D. B., M. G. Schlax, S. K. Esbensen, N. Thum, M. H. Freilich, F. J. Wentz, C. L. Gentemann, and M. J. McPhaden, 2001: Observations of coupling between surface wind stress and sea surface temperature in the eastern tropical Pacific, *J. Climate14*, 1479-1498.

Chelton, D. B., F. J. Wentz, C. L. Gentemann, R. A. de Szoeke, and M. G. Schlax, 2000: Microwave SST observations of transequatorial instability waves, *Geophys. Res. Lett.*, *27*, 1239-1242.

Deser, C. , J. J. Bates, and S. Wahl, 1993: The influence of sea surface temperature gradients on stratiform cloudiness along the equatorial front in the pacific ocean, *J. Climate*, 1172-1180.

Fairall, C. W., E. F. Bradley, J. S. Godfrey, G. A. Wick, J. B. Edson, and G. S. Young, 1996: Cool-skin and warm-layer effects on sea surface temperature, *J. Geophys. Res.*, *101*, 1295-1308.

Friehe, C. A., W. J. Shaw, D. P. Rogers, K. L. Davidson, W. G. Large, S. A. Stage, G. H. Cresenti, S. J. S. Khalsa, G. K. Greenhut, and F. Li, 1991: Air-sea fluxes and surface layer turbulence around a sea surface temperature front, *J. Geophys. Res.*, *96*, 8593-8609.

Grachev, A. A., and C. W. Fairall, 1997: Dependence of the Monin-Obukhov stability parameter on the bulk Richardson number over the ocean, *Journal of applied Meteorology*, *36*, 406-414.

Grachev, A. A., C. W. Fairall, and E. F. Bradley, 2000: Convective profile constants revisited, *Boundary-Layer Meteorology,3*, 495-515.

Hashizume, H. , S.-P. Xie, W. T. Liu, and K. Takeuchi 2000: Local and remote atmospheric response to tropical instability waves: A global view from space, *J. Geophys. Res.*, submitted.

Hayes, S. P., M. J. McPhaden, and J. M. Wallace, 1989: The influence of sea-surface temperature on surface wind in the eastern equatorial Pacific: Weekly to monthly variability, *J. Climate*, *2*, 1500-1506.

Horel, J. D.,1984: Complex principal component analysis: theory and examples. *Climate Appl. Meteor.*, *23*, 1660-1673.

Kummerow, C., W. Barnes, T. Kozu, J. Shiue, and J. Simpson, 1998: The Tropical Rainfall Measuring Mission (TRMM) Sensor Package, *J. Atmos. Ocean Technol.*, *15*, 808-816.

Lindzen, R. S., and S. Nigam, 1987: On the role of sea surface temperature gradients in forcing low-level winds convergence in the tropics, *J. Atmos. Sci.*, *44*, 2418-2436.

Liu, W. T., X. Xie, P. S. Polito, S.-P. Xie, and H. Hashizume, 2000: Atmospheric manifestation of tropical instability wave observed by QuickSCAT and Tropical Rain Measuring Mission, *Geophys. Res. Lett.*, *27*, 2545-2548.

McPhaden, M. J., A. J. Busalacchi, R. Cheney, J. R. Donguy, K. S. Gage, D. Halpern, M. Ji, P. Julian, G. Meyers, G. T. Mitchum, P. P. Niiler, J. Picaut, R. W. Reynolds, N. Smith, and K. Takeuchi, 1998: The tropical ocean-global atmosphere (TOGA) observing system: a decade of progress, *J. Geophys. Res.*, *103*,14169-14240.

Mitchell, T. P., and J. M. Wallace, 1992: The annual cycle in Equatorial Convection and sea surface temperature, *J. Climate*, *5*, 1140-1156.

Oppenheimer, A. V., and R. A. Schafer, 1975: *Digital Signal Processing. Prentice Hall*, 360pp.

Paluch, I. R., G. McFarquhar, D. H. Lenschow, and Y. Zhu, 1999: Marine boundary layer associated with ocean upwelling over the eastern equatorial Pacific ocean, *J. Geophys. Res.*, *104*, 30913-30936.

Philander, S. G. H., D. Gu, D. Halpern, G. Lambert, N.-C. Lau, T. Li, and R. C. Pacanowski, 1996: Why the ITCZ is mostly north of the equator, *J. Climate*, *9*, 2958-2972.

Qiao, L., and R. H. Weisberg, 1995: Tropical instability wave kinematics: Observations from the Tropical Instability Wave Experiment, *J. Geophys. Res.*, *100*, 8677-8693.

Sweet, W., R. Fett, J. Kerling, and P. LaViolette, 1981: Air-sea interaction effects in the lower troposphere across the north wall of the gulf stream, *Mon. Wea. Rev.*, *109*, 1042-1052.

Tomas, R. A., and P. J. Webster, 1997: The role of inertial instability in determining the location and strength of near-equatorial convection, *Quart. J. Roy. Meteor. Soc.*, *123*, 1445-1482.

Tomas, R. A., J. R. Holton, and P. J. Webster, 1999: The influence of cross-equatorial pressure gradients on the location of near-equatorial convection, *Quart. J. Roy. Meteor. Soc.*, *125*, 1107-1127.

Wai, M. M.-K.,and S. A. Stage, 1989: Dynamical analysis of marine atmospheric boundary layer structure near the Gulf Stream oceanic front, *Quart. J. Roy. Meteor. Soc.*, *115*, 29-44.

Wallace, J. M., T. P. Mitchell, and C. Deser, 1989: The influence of sea-surface temperature on surface wind in the eastern equatorial Pacific: Seasonal and interannual variability, *J. Climate*, *2*, 1492-1499.

Waliser, D. E., and R. C. J. Somerville, 1994: Preferred latitudes of the intertropical convergence zone, *J. Atmos. Sci.*, *51*, 1619-1639.

Wang, B., and Y. Wang, 1999: Dynamics of the ITCZ-equatorial cold tongue complex and causes of the latitudinal climate asymmetry, *J. Climate*, *12*, 1830-1847.

Xie, S.-P., M. Ishiwatari, H. Hashizume, and K. Takeuchi, 1998: Coupled ocean-atmospheric waves in the equatorial front, *Geophys. Res. Lett.*, *25*, 3863-3866.

Zhang, G. J., and M. J. McPhaden, 1995: The relationship between sea surface temperature and latent heat flux in the equatorial Pacific, *J. Climate*, 589-605.

APPENDIX

Extended Literature Survey

The region of interest from the equator to 5° N is characterized by large SST gradients and strong air-sea interactions and plays an important role in the cold tongue-ITCZ complex. The region affects the structure of the ITCZ inflow and is a forcing for the upper ocean through wind stress and heat flux.

Both large and small scale air-sea interaction processes are is important for this region. The boundary conditions for the ABL response across the SST-front are set up by the large scale dynamics which are influenced by the cross-equatorial pressure gradient, large scale SST distribution, the trade winds and their convergence into the ITCZ. The ABL response itself takes place on smaller scales, where frontal SST gradients, local pressure adjustments and turbulent momentum transport become important. This section is therefore divided into a large scale and small scale part, discussing the scale depending aspects that effect and control the region of interest.

Prior investigations of large-scale dynamics in the region have used model and observational approaches to explain the location of the ITCZ off the equator. In a series of publications (Lindzen and Nigam (1987), Mitchell and Wallace (1992), Philander et al. (1996), Tomas and Webster (1997), Tomas et al. (1999) Wang and Wang (1999), and others) several interaction and feedback mechanisms have been proposed and refined.

Lindzen and Nigam (1987) used a simple one-layer model of the trade cumulus layer to show the significance of pressure gradients directly generated by SST distributions for the production of low-level moisture convergence.

On the basis of observational evidence Mitchell and Wallace (1992) argued that the increase in the northward surface wind in response to the onset of the northern summer monsoon brings colder water to the surface to form and intensify

the equatorial cold tongue. A local pressure adjustment to the SST distribution increases the northward directed pressure gradient force just north of the cold tongue and the eastward directed pressure gradient force along the equator to the west of the cold tongue. Both pressure gradients act as positive feedbacks which intensify upwelling favorable winds to the north and to the west of the cold tongue.

The linear shallow-water theory and a moist primitive equation model were examined by Waliser and Sommerville (1994). They noted that low-level convergence and latent energy support is dynamically maximized some 4 to 12 degrees off the equator.

Another combination of mechanisms was proposed by Philander et al. (1992) from the analysis of a coupled atmosphere-ocean model. They suggest that the coastal geometry and the prevailing surface winds can produce coastal upwelling. The upwelling and associated lowering of the SST will be more pronounced south than north of the equator because of the inclination of the coast lines to the meridians. The initial asymmetry could be maintained by low-level stratus clouds over the cold waters.

In other large scale model approaches Tomas and Webster (1997) and Tomas et al. (1999) used a different explanation for the northward displacement of the ITCZ. They argued that in the presence of a cross equatorial pressure gradient the displacement of absolute vorticity into the northern hemisphere is responsible for the preferred location of the ITCZ. In their model analysis they found evidence that the displacement leads to inertial instability and a convergence-divergence doublet, which is sufficient to explain the location of the ITCZ. The follow up study by Tomas et al. (1999) was able to show that in the linear model the flow does not meet the linear stability criteria. However, the full nonlinear model

found a range of values where the response to the forcing is highly nonlinear. A large increase in meridional wind was found for small changes in the pressure gradient. To explain the atmospheric response to TIW SST patterns such as those seen in Fig. 1.1, two classes of hypotheses have been proposed: one where *ABL adjustments and air-sea interactions* are responsible for the observed acceleration of surface wind and the other where wind acceleration is associated with the *ABL pressure adjustments* to the SST distribution.

In the context of the equatorial TIWs, Wallace et al. (1989) hypothesized that the ABL destabilization and increased vertical momentum mixing over the SST front are responsible for the observed acceleration of surface wind. Bond (1992) found that the ABL vertical wind shear over the SST front was reduced. A similar mechanism was proposed by Sweet et al. (1981) to explain changes in sea state and wind pattern across the Gulf Stream SST front. Because the downward momentum mixing reduces the vertical shear in the lower part of the boundary layer, this mechanism will hereafter be referred as the *ABL momentum mixing hypothesis.*

On larger scales, the SST distribution of cold surface water along the equator and warm surface north of the equator can be associated with high and low ABL pressure anomalies, respectively. These pressure anomalies associated with the SST distribution persist throughout the ABL and induce wind accelerations. Lindzen and Nigam (1987) proposed this mechanism to explain the large-scale patterns of convergence and wind forcing in the tropics. If we apply this mechanism to explain the ABL response to the smaller scale SST disturbances caused by TIWs, the resulting wind patterns differ from the patterns expected from the ABL momentum mixing hypothesis (Hayes et al. 1989).

In addition, the model analysis by Wai and Stage (1989) suggests that the vertical structure of the ABL pressure adjustments over the SST front may be important, giving rise to a secondary circulation, similar to a land-sea wind circulation. Increased (decreased) pressure is expected in the lower part of the ABL over cold (warm) water, while the opposite is expected in the upper portion. The pressure distribution causes a thermally direct circulation in a vertical plane perpendicular to the SST front. Wai and Stage found that this mechanism can result in increased surface wind stress over the SST front through differential ABL pressure adjustments rather than direct momentum flux convergence patterns.

In an observational study of boundary layer structure across the SST-front Paluch et al. (1999) observed an increase of wind speed 61 m above the cold tongue accompanied with a decrease of whitecaps and a relaxing of wind speed to its previous (warm water) value after the transition back to warm surface water. The observed wind speed values at 61 m and the changes in sea state are consistent with argumentation of enhanced vertical mixing of momentum and reduced vertical shear over warm water, and inhibited mixing with increased shear over cold water.

The regional atmospheric response to TIWs based on weekly averages of wind and SST estimates was analysed by Xie et al. (1998) using satellite data and a coarse resolution atmospheric general circulation model. The observational results indicate that the SST distribution induces wind convergence and divergence patterns that are consistent with the ABL momentum mixing hypothesis. The model results indicate that the TIW induced surface wind perturbations penetrate to at least 800 hPa and that the surface wind field may force a deep atmospheric response.

The remote contribution of TIW to the variability of the ITCZ is shown by Hashizume et al. (2001). The patterns of water vapor, liquid water and rain north of 6°N are shifted towards the west relative to the pattern of SST. Increased water vapor, liquid water and rain are found in regions of wind convergence. Additionally, they found that the momentum mixing mechanism and the pressure adjustment mechanism are equally important for the region between the equator and 4°N.

With the availability of high resolution satellite wind and SST data, Chelton et al. (2001) demonstrated the consistency of the ABL momentum mixing hypothesis with the observed TIW wind stress and SST patterns. The ABL momentum mixing mechanism for SST modification of the surface wind field is most clearly manifested in the dependency of the wind stress divergence and curl fields on the angle between the SST gradient vector and the wind stress. They found that the wind stress divergence has a cosine dependency while the wind stress curl has a sine dependency. In other words, the wind stress divergence and curl are proportional to the downwind and cross wind components of the SST gradient, respectively. As described by Hayes et al. (1989) the ABL momentum mixing hypothesis requires a distinct phase relation between SST and the wind components. SST perturbations should be in phase with the meridional wind component and wind speed, but should out of phase with the zonal component. Liu et al. (2000) verified this phase relationship.

There has been observational and theoretical evidence that the ABL momentum mixing hypothesis is the principle coupling mechanism across the equatorial SST front. However, the simultaneous existence of a coupling as found by Wai and Stage has not been considered in the equatorial region. It seems possible that a combination of both mechanism is acting to produce the observed surface

wind pattern. The thermal direct circulation could provide additional horizontal momentum which is mixed and transported vertically to accelerate surface winds. In this manner vertical shear is reduced throughout the boundary layer.